Resolution Requirements for the Numerical Computation of Tonal Noise in Compressors and Turbines of Aeroengines

T. Hüttl[1], G. Kahl, F. Kennepohl and K. Heinig
MTU Aero Engines GmbH
Dachauer Strasse 665
D-80995 München, Germany

Abstract

The time linearized Euler method Lin3D is applied to two sets of test cases. 2D wave propagation test cases in homogeneous flow are used to quantify numerical dissipation and dispersion of the discretization scheme. The minimum number of mesh diagonals between two wave fronts has been found to be an appropriate measure of the resolution of a wave. Correlations have been found that characterize the dissipation and dispersion behavior of the code and therefore the resolution requirements for a given flow simulation. The transmission and reflection of plane sound waves incident upon a single cascade of finite plates has also been calculated with Lin3D and compared with an analytical method of Koch [5]. The computed ratios of transmitted or reflected to incident pressure wave amplitude agree well with the analytical solution, even for scattered modes.

1. Introduction

The noise produced by jet engines has become one of the major concerns in today's pollution- and noise-conscious society. The jet-exhaust noise has been reduced significantly with the increasing by-pass ratios of modern turbofan engines. But now, the pure tonal noise, produced by rotor-stator interaction in compressors and turbines can become a dominant source of engine noise. Together with the noise generation and radiation, the sound transmission through blade rows in axial-flow turbomachines is also of great importance. Various calculation methods ranging from analytic methods for simplified flow and geometry, over empirical methods based on correlations calibrated by experimental data, to the wide range of numerical methods have been established within the aeroacoustic design process of turbomachines.

In this paper, we focus on a numerical calculation method, based on the time linearized Euler equations. This CFD code Lin3D developed at MTU is already used for aeroelastic design of aeroengine compressors and turbines. It may also be applied to the aeroacoustic design of these engine components. In contrast with analytical methods a more realistic description of blade and duct geometry is possible. Compared with Navier-Stokes methods, the computational requirements of Lin3D are much smaller. Before applying a code to a new kind of problems, its requirements and weaknesses have to be studied. It is the aim of the present study to investigate the resolution requirements of Lin3D for aeroacoustic computations.

First, the wave propagation in homogeneous flow has been computed in order to quantify the effect of numerical dissipation and dispersion on the solution. Then, the problem of the transmission of a sound wave through a blade row has been solved where the accuracy of the code can be benchmarked with an analytical method.

[1] Author for correspondence:
Dr. Thomas Hüttl, MTU Aero Engines GmbH, Abt. TPAI,
Dachauer Strasse 665, D-80995 München, Germany
Tel.: +49-(0)89-14 89-68 36 ; Fax: +49-(0)89-14 89-95242 ; Email: Thomas@Huettl.de

Paper presented at the RTO AVT Symposium on "Ageing Mechanisms and Control: Part A – Developments in Computational Aero- and Hydro-Acoustics", held in Manchester, UK, 8-11 October 2001, and published in RTO-MP-079(I).

2. Numerical Method

The CFD code Lin3D is a time-linearized Euler method for 3D cascade flows [2,3,4]. The unsteady flow is assumed to be a small harmonic perturbation of the non-linear steady flow, so that the steady flow problem is decoupled from the unsteady problem. As long as the wave amplitudes remain moderate, the higher order terms in the governing equations derived under this assumption can be neglected and the describing unsteady flow equations become linear. The small-disturbance Euler equations are transformed into the frequency domain, so that the results are given as amplitudes and phases of the flow variables in the whole (3D) computational domain.

The base flow for the time linearized Euler code has been prescribed analytically for the investigations discussed here, but it can be the result of a steady 3D Euler computation, as well. Lin3D is restricted to small disturbances of the mean, inviscid, steady flow and its applicability is limited to cases with (predominantly) attached flow. The code is based on the linearization of the steady Euler method described in [1] and is an extension of the code described in [2,4].

Lin3D uses a Finite-Volume scheme with a 3-step Runge-Kutta time integration method. A structured H-type mesh with node centered variable arrangement is required to describe the geometry of the flow domain.

Lin3D has proven to be sufficient for most cases concerned with turbines. It is a fast and robust tool routinely used in the design process to assess flutter stability and forced response of compressor and turbine bladings. It features deforming meshes, non-reflecting boundary conditions, arbitrary eigenmodes (including chordwise bending), forced-response calculations for generalized forces due to up- and downstream disturbances and the possibility of calculation of acoustic modes. Lin3D runs on a wide variety of platforms ranging from workstations to multiprocessor vector supercomputers, with the option of parallel computing to speed up the turnaround times.

3. Wave propagation in homogeneous flow

3.1 Computational domain and setup

The accuracy of the code for wave propagation in homogeneous 2D flow has been tested for numerous upstream and downstream propagating waves. For each single test case the same equidistant mesh has been used, where the vector of the homogeneous mean flow is parallel to the mesh lines, see Figure 3.1. Physical and geometrical parameters of the cases are listed in Table 3.1. In order to realize a plane 2D flow with the 3D code in cylindrical coordinates, a small ratio of channel height ($r_{tip} - r_{hub} = 0.2m$) to tip radius ($r_{tip} = 300m$) has been chosen and discretized by 4 mesh cells.

Table 3.1: Physical and geometrical parameters of 2D wave propagation calculations.

$L = 1.5m$	$N_x = 60$	$p_s = 85.15kPa$
$T = 1.0m$	$N_y = 40$	$\mathrm{Ma} = 0.5$
$\beta_s = 60°$	$a = 332.0\frac{m}{s}$	$T_s = 274.3K$

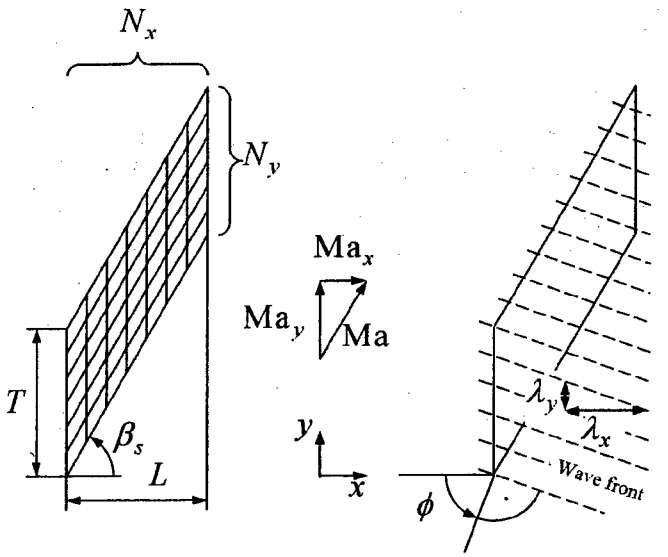

Figure 3.1: Flow domain of 2D wave propagation calculations (without blades).

Two parameters are varied, the circular frequency ω and the incidence angle ϕ of the pressure wave:

$$\omega_A = 0.25\frac{\pi a}{T},\ \omega_B = \frac{\pi a}{T},\ \omega_C = 4\frac{\pi a}{T},\ \omega_D = 16\frac{\pi a}{T}$$

$$\phi = 0°,15°,30°,45°,\_\_,345° \quad \text{(not: } 90°,270°\text{)}.$$

For upstream traveling waves ($90° < \phi < 270°$) the boundary conditions for a pressure perturbation have to be specified at the outlet plane; for downstream traveling waves ($0° \le \phi < 90°$ and $270° < \phi < 360°$) at the inlet plane. All waves are sinusoidal in the y-direction. The amplitudes are sufficiently small, so that non-linear effects can be neglected (peak to mean pressure variation of 0.1% of the static pressure).

3.2 Resolution of the waves

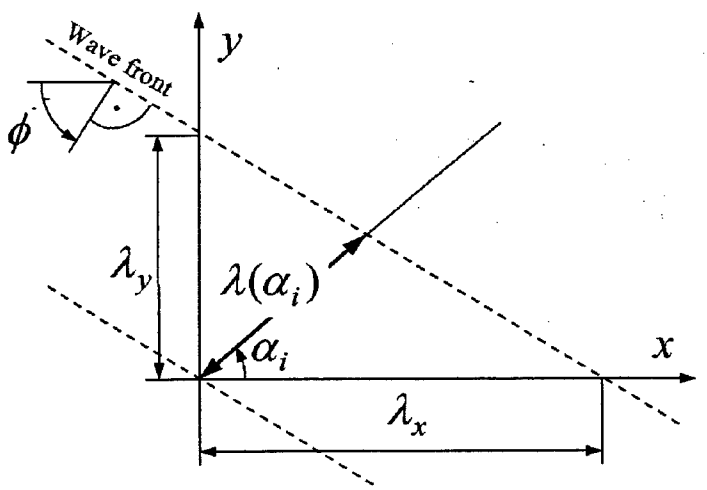

Figure 3.2: Geometry of 2D waves.

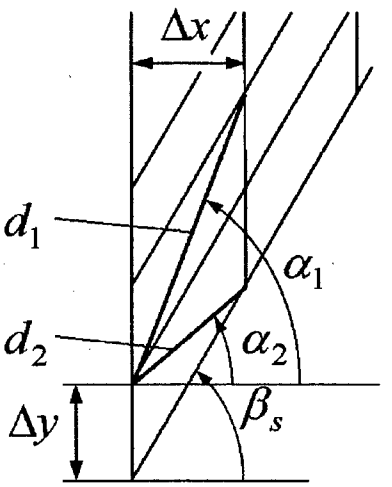

Figure 3.3: H-type mesh geometry.

Although mean flow, flow domain, number of mesh points N_x, N_y and wave number

$$k = \frac{\omega}{a}$$

are chosen to be identical for constant ω, the resolution of the waves is not equal for the simulation, as it depends on the incident angle ϕ. However, the wave lengths λ also depend on ϕ for flow at $Ma \neq 0$. A characteristic quantity for the resolution R in discrete domains is the minimum number of mesh cell diagonals between two wavefronts:

$$R = \min\left(\frac{\lambda(\alpha_1)}{d_1}; \frac{\lambda(\alpha_2)}{d_2}\right) .$$

$\lambda(\alpha_i)$ is the distance between two wavefronts along a line under an angle of α_i to the horizontal axis, see Figure 3.2.

$$\lambda(\alpha_i) = \frac{\lambda_x}{\cos\alpha_i + \tan\phi \sin\alpha_i} .$$

λ_x can be obtained from

$$\lambda_x = \frac{2\pi c_x}{\omega} \text{ , using } c_x = a\,\mathrm{Ma}\cos\beta_s + \frac{a}{\cos\phi} + a\,\mathrm{Ma}\sin\beta_s \tan\phi .$$

Two diagonals d_1 and d_2 exist in a structured H-type mesh (Figure 3.3). Their lengths and their angles α_1, α_2 are defined by

$$d_1 = \sqrt{\Delta x^2 + (\Delta x \tan\beta_s + \Delta y)^2} \text{ , } \tan\alpha_1 = \tan\beta_s + \frac{\Delta y}{\Delta x} ,$$

$$d_2 = \sqrt{\Delta x^2 + (\Delta x \tan\beta_s - \Delta y)^2} \text{ , } \tan\alpha_2 = \tan\beta_s - \frac{\Delta y}{\Delta x} \text{ , with } \Delta x = \frac{L}{N_x},\ \Delta y = \frac{L}{N_y} .$$

3.3 Results

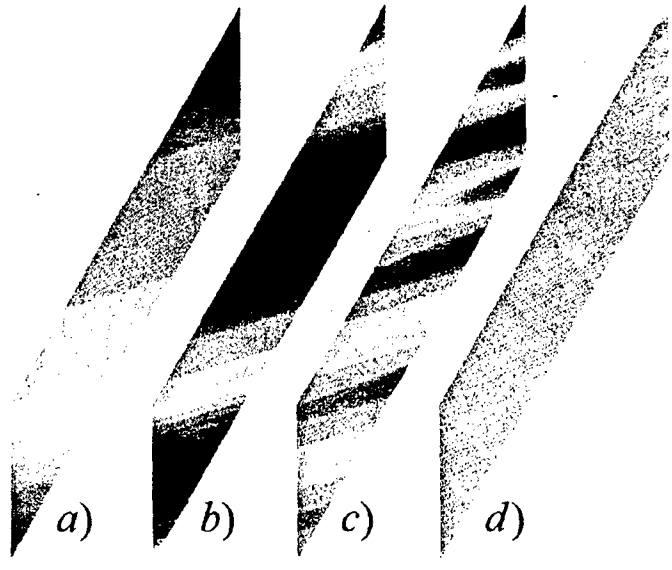

Figure 3.4: Unsteady pressure for four wave propagation test cases with the same incident angle $\phi = 105°$ and different circular frequency ω: a) ω_A, b) ω_B, c) ω_C, d) ω_D.

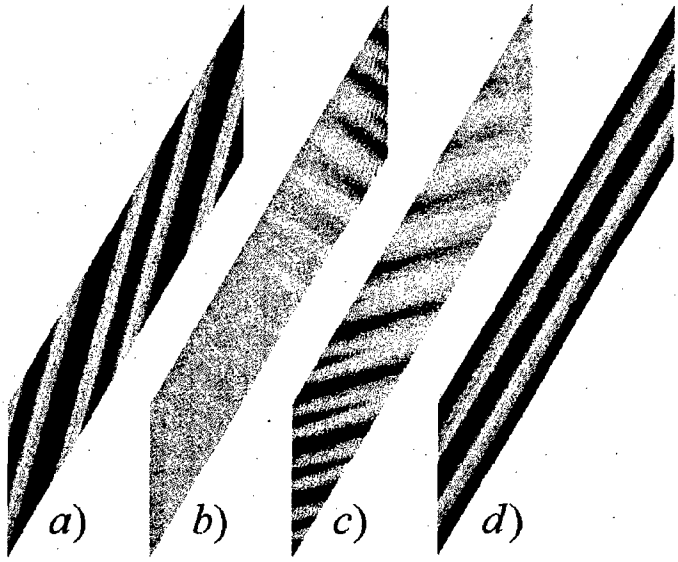

Figure 3.5: Unsteady pressure for four wave propagation test cases with the same circular frequency ω_C and different incident angle ϕ: a) $\phi = 165°$, b) $\phi = 225°$, c) $\phi = 285°$, d) $\phi = 330°$.

A first impression of the wave propagation in a 2D flow field is given in Figures 3.4 and 3.5. Figure 3.4 demonstrates that the damping of the waves increases for higher ω (smaller k, lower R). In Table 3.2, the values of the resolution R for four cases with the same circular frequency ω_C, plotted in Figure 3.5, are listed. This Figure shows that the damping depends on the resolution R, which is a function of the incident angle ϕ of the wave.

The purpose of the wave propagation test cases is to analyze, how strong numerical dissipation and numerical dispersion can affect the flow solution. Numerical dissipation and dispersion are unwelcome side effects of a discrete solution method and depend on the discretization scheme of the code. Numerical dissipation leads to the exponential decrease of the wave amplitudes $A(x)$ in (horizontal) propagation direction and can be quantified by the decay rate Dec

$$Dec = -20 \cdot \log_{10}\left(\frac{A(x+\Delta x)}{A(x)}\right) \qquad \text{for a downstream propagating wave}$$

$$Dec = -20 \cdot \log_{10}\left(\frac{A(x-\Delta x)}{A(x)}\right) \qquad \text{for an upstream propagating wave}$$

Numerical dispersion leads to an incorrect propagation velocity of a wave or to a change in its propagation direction. Dispersion can be quantified by the phase change error Pce, the difference between analytical $P_a(x)$ and numerical phase $P_n(x)$ change

$$Pce = \left|\left(P_n(x+\Delta x) - P_n(x)\right) - \left(P_a(x+\Delta x) - P_a(x)\right)\right|$$

Table 3.2: Resolution of the pressure waves of the four test cases in Figure 3.5.

Case	a	b	c	d
Incident angle	$\phi = 165°$	$\phi = 225°$	$\phi = 285°$	$\phi = 330°$
Resolution	$R = 22.4$	$R = 3.92$	$R = 5.43$	$R = 40.0$

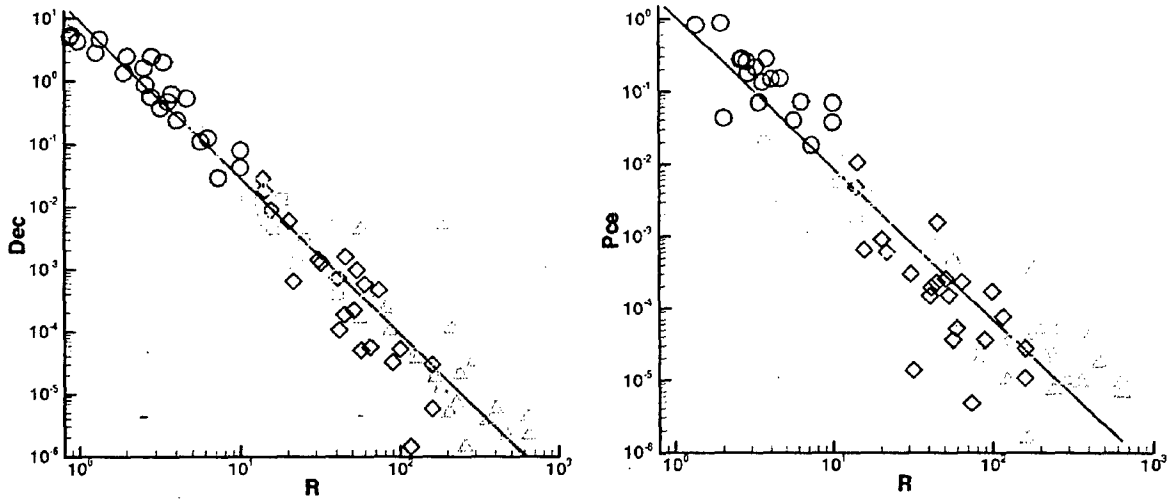

Figure 3.6: Decay rate *Dec* (left) and phase change error *Pce* (right) of the wave propagation test cases drawn over the resolution R: △ ω_A, ◇ ω_B, ω_C, ○ ω_D, lines: $Dec_{lq} = 9.2 \cdot R^{-2.5}$ or $Pce_{lq} = 1.1 \cdot R^{-2.1}$.

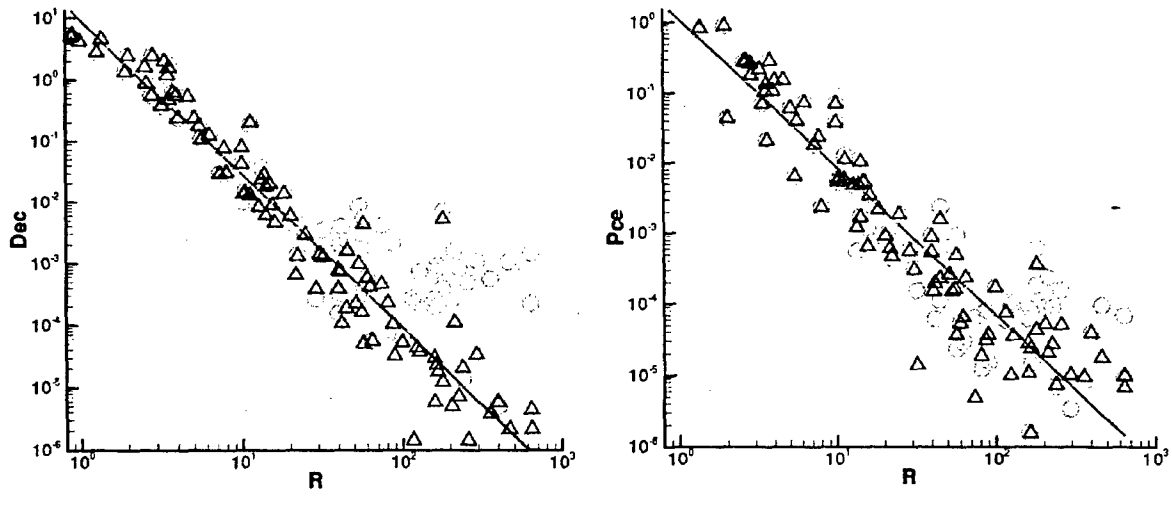

Figure 3.7: Decay rate *Dec* (left) and phase change error *Pce* (right) of the wave propagation test cases drawn over the resolution R for two different convergence criteria: △ low convergence criterium ($\mathrm{Res}_\rho = 5 \cdot 10^{-7}$), ○ high convergence criterium ($\mathrm{Res}_\rho = 5 \cdot 10^{-5}$), lines: $Dec_{lq} = 9.2 \cdot R^{-2.5}$ or $Pce_{lq} = 1.1 \cdot R^{-2.1}$.

In Figures 3.6 and 3.7, the decay rates and the phase change errors of the wave propagation test cases are drawn over the resolution R (section 3.2). Obviously, *Dec* and *Pce* are both correlated with R: With decreasing R, the decay rate and the phase change error and therefore numerical dissipation and dispersion increase.

When analysing *Dec* and *Pce* for different ω, it is not astonishing, that cases with higher frequency ω (smaller k) are worse resolved. Nevertheless, the symbol clouds for constant ω overlap with other distributions, because the incident wave angle ϕ has a remarkable effect on the resolution. Values of R for constant ω can even differ by one order of magnitude.

Using logarithmic scales on both axes, most of the plotted values are close to a straight line ($y = a \cdot R^b$). The parameters a, b can be obtained by the least squares method:

$$Dec_{lq} = 9.2 \cdot R^{-2.5}$$
$$Pce_{lq} = 1.1 \cdot R^{-2.1}$$

From linear theory for a 2nd order CFD code on a uniform mesh it is expected, that a 3rd order relationship exists between the decay rate and the resolution [6] and a 2nd oder relationship between the phase change error and the resolution. Better agreement with the 3rd order decay is achieved, if only cases B,C and D are used for the least squares fit ($Dec_{lq} = 14.9 \cdot R^{-2.8}$). The results of cases A might be influenced by the convergence criterion (density residual Res_ρ) of the code. This is demonstrated in Figure 3.7, where simulations with good convergence criterion are compared with simulations with worse convergence criterion: For higher R, the values of Dec and Pce deviate significantly from the least squares fit of the good convergence criterion. For a smaller (better) convergence criterion the cases with lower R are almost uninfluenced, but the values of Dec and Pce for higher R come closer to the correlation function.

Dec and Pce represent the accuracy of the calculation of a wave within the size of one mesh cell Δx. They define minimum requirements for the resolution of a pressure wave. As an example: if the decrease of the pressure amplitude by 1dB (0.1dB) due to numerical dissipation after 200 mesh cells Δx is assumed to be acceptable, we obtain $Dec = 5 \cdot 10^{-3}$ $\left(5 \cdot 10^{-4}\right)$ and need a resolution of the wave of $R = 20$ (50).

4. Interaction of plane waves with flat plates

4.1 Geometry and settings

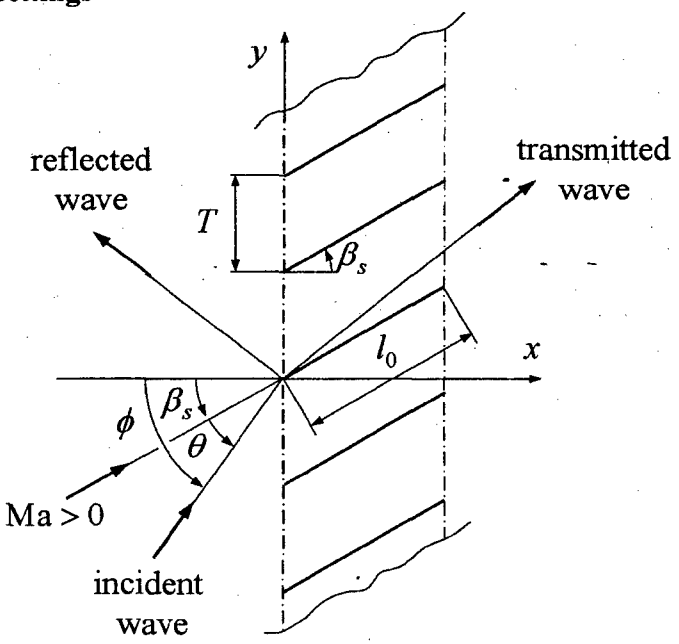

Figure 4.1: Geometry of the flat plate test cases.

In this section, the transmission and reflection of plane sound waves incident upon a single cascade of finite plates is studied. This problem, including scattering, has been solved by Koch [5] by means of the finite Wiener-Hopf technique. These analytical results will be used for comparison with computations using Lin3D.

A single cascade of parallel flat plates of length $l_0 = 1m$, staggered at an angle $\beta_s = 60°$ and at zero angle of attack, is considered and is shown in Figure 4.1. ϕ and $\theta = \phi - \beta_s$ are two different definitions of the angle of the incident wave. For the computation, the regions in front of the cascade, L_f, and behind it, L_b, both have an axial extension of $L_f = L_b = 0.5m$. Two circular frequencies have been studied: $\omega_A = 0.25\pi a \frac{1}{T}$ as a sub-resonant example and $\omega_B = \pi a \frac{1}{T}$ as a super-resonant example, where scattered modes appear. Only cut-on modes are considered. For other physical, geometrical and numerical parameters, the same values have been chosen as for the wave propagation test cases in section 3.

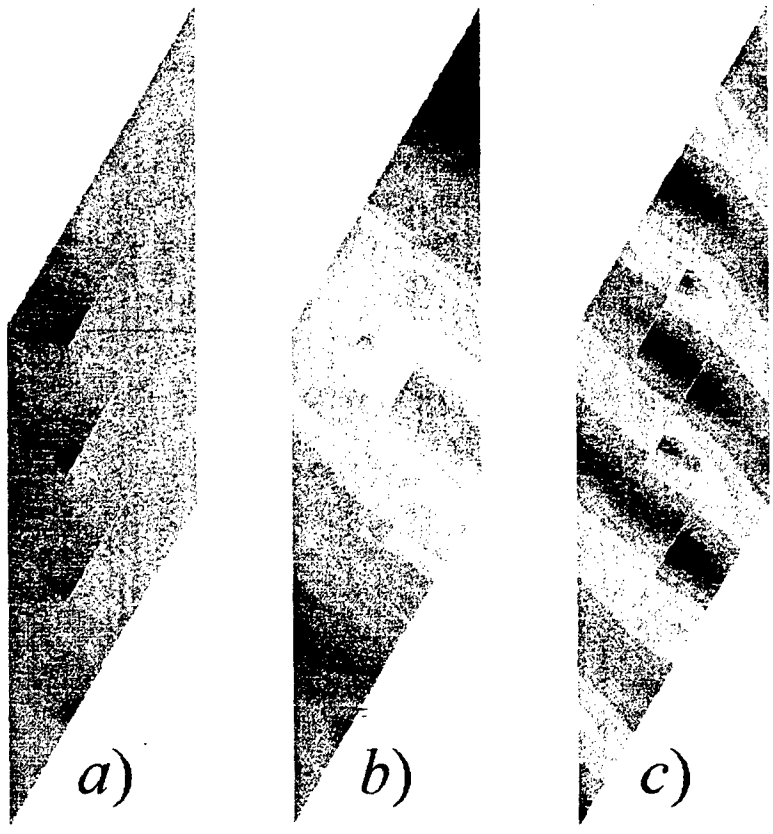

Figure 4.2: Unsteady pressure for three flat plate test cases: a) ω_A, $\phi = 345°$, b) ω_A, $\phi = 225°$, c) ω_B, $\phi = 225°$.

4.2 Sub-resonant test cases

The incident waves interact with the blades, when passing through a blade row. If the blades are perpendicular to the wave front, the wave is completely transmitted. For blades that are parallel to wave fronts, the waves are almost completely reflected (Close to this point, full reflection appears for a certain angle depending on the Mach number). In general, the incident acoustic

wave is partially reflected and partially transmitted through the blade row. For the sub-resonant test case, where mode scattering does not appear, two snap-shots of the pressure field are shown in Figures 4.2 a) and b).

For six representative cases, some parameters can be found in Table 4.1. Beside the incident wave angles ϕ, θ, the wave numbers k, k_x, k_y and the wave lengths λ, λ_x, λ_y are listed:

$$k=\frac{\omega}{a},\ k_x=\frac{\omega}{c_x},\ k_y=k_x\tan\phi,\ \lambda=\sqrt{\frac{\lambda_x^2\lambda_y^2}{\lambda_x^2+\lambda_y^2}},\ \lambda_x=\frac{2\pi}{k_x},\ \lambda_y=\frac{2\pi}{k_y}$$

Waves with a cut-off ratio $|\xi|>1$ are cut-on (propagating waves), while waves are cut-off (exponentially decaying) for $|\xi|<1$.

Table 4.1: Parameters of some of the sub-resonant flat plate test cases.

θ	ϕ	k	k_x	k_y	λ	λ_x	λ_y	ξ	$\lvert p_0^t\rvert/\lvert p_0^i\rvert$	$\lvert p_0^r\rvert/\lvert p_0^i\rvert$
75°	135°	0.785	-0.492	0.492	9.035	-12.778	12.778	1.140	0.4477	0.0885
120°	180°	0.785	-1.047	0.000	6.000	-6.000	∞	∞	0.6147	0.2820
165°	225°	0.785	-1.074	-1.074	4.137	-5.850	-5.850	1.366	0.9108	0.2284
255°	315°	0.785	0.638	-0.638	6.965	9.850	-9.850	2.300	0.5313	0.4769
300°	360°	0.785	0.628	0.000	10.00	10.000	∞	∞	0.7641	0.4700
345°	45°	0.785	0.374	0.374	11.86	16.778	16.778	1.497	0.9763	0.1606

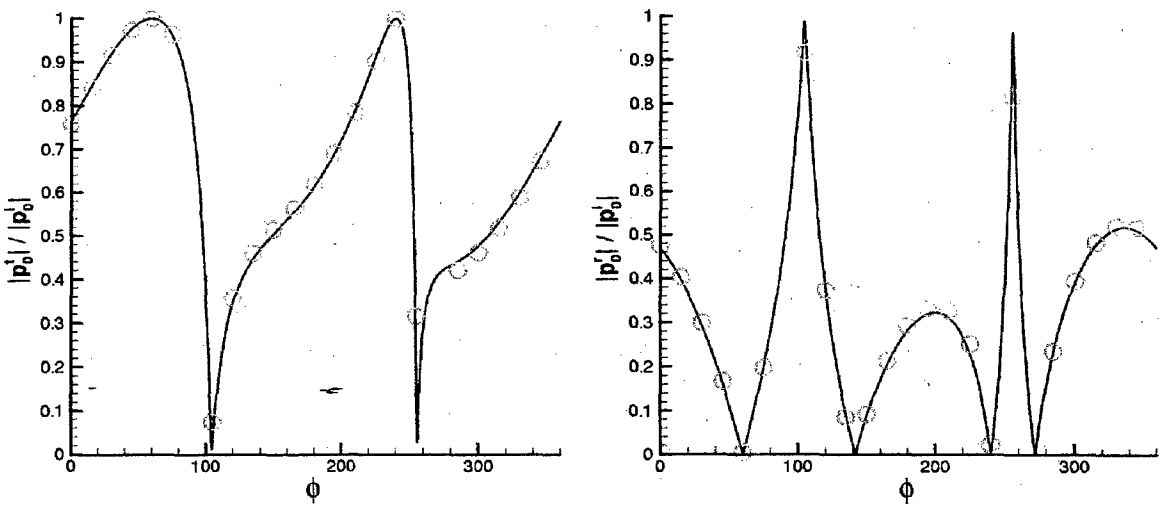

Figure 4.3: Variation of transmitted (left) and reflected pressures (right) with incidence angle for the sub-resonant cases: Lines: analytical solution [5], ○ Lin3D.

The cut-off ratio ξ is also shown in Table 4.1:

$$\xi=\begin{cases}\dfrac{1}{\mathrm{Ma}_y+\sqrt{1-\mathrm{Ma}_x^2}}\dfrac{k}{k_y} & k_y>0\\[2ex] \dfrac{1}{\mathrm{Ma}_y-\sqrt{1-\mathrm{Ma}_x^2}}\dfrac{k}{k_y} & k_y<0\end{cases}$$

Furthermore, the (analytic) ratios of transmitted p_0^t or reflected p_0^r wave amplitudes to the amplitudes of the incident pressure wave p_0^i are listed for the six cases in Table 4.1.

The variations of these ratios $|p_0^t|/|p_0^i|$ and $|p_0^r|/|p_0^i|$ with incidence angle ϕ are drawn in Figure 4.3. A maximum transmission ratio $|p_0^t|/|p_0^i|=1$ is obtained for the two wave directions, where the upstream or downstream wave fronts are perpendicular to the blades ($\phi = 60°, 240°$). These maxima are correlated with minima of the reflection ratio $|p_0^r|/|p_0^i|=0$. Analytical and numerical results agree well with each other within the whole range of ϕ.

4.3 Super-resonant test cases

Scattered pressure waves ($m \neq 0$) are generated, when a pressure wave interacts with a cascade. For some of the cases with higher circular frequency $\omega_B = \pi a \frac{1}{T}$ scattered modes can be cut-on:

$m=-1$ is cuton for $10° < \phi < 174°$
$m=1$ is cuton for $223° < \phi < 294°$

Therefore the cases with this frequency are called super-resonant. A snap-shot of the pressure field of one super-resonant case is shown in Figure 4.2 c). The variation of the ratios $|p_m^t|/|p_m^i|$, $|p_m^r|/|p_m^i|$ with incidence angle ϕ is drawn in Figure 4.4. Here again, analytical and numerical results agree well with each other within the whole range of ϕ.

5. Summary

The application of the time-linearized Euler method Lin3D to 2D wave propagation problems in homogeneous flow shows the dependency of numerical errors with the mesh resolution. For skewed meshes, the minimum number of mesh diagonals between two wave fronts is an appropriate measure for the mesh resolution. Numerical errors of the discretization scheme in form of numerical dissipation and numerical dispersion increase for increasing frequency at constant mesh. For constant frequency, the resolution of a wave depends on the angle of the incident wave and varies within one order of magnitude. The angle of the incident wave has therefore a significant effect on numerical errors. Correlations, calibrated with the simulations, can be used further to check the mesh size before performing simulations with Lin3D.

In a second study, the transmission and reflection of plane sound waves incident upon a single cascade of finite plates has been calculated with Lin3D. Computed results have been compared with an analytical method of Koch [5]. It has been looked at sub-resonant test cases and at super-resonant cases, where cut-on scattered modes appear. The computed ratios of transmitted or reflected to incident pressure wave amplitude agree well with the analytical solution. Even the ratios for scattered modes can be predicted accurately with Lin3D.

As a next step, the simulation of more realistic test cases with finite blade thickness, or 3D flow is envisaged.

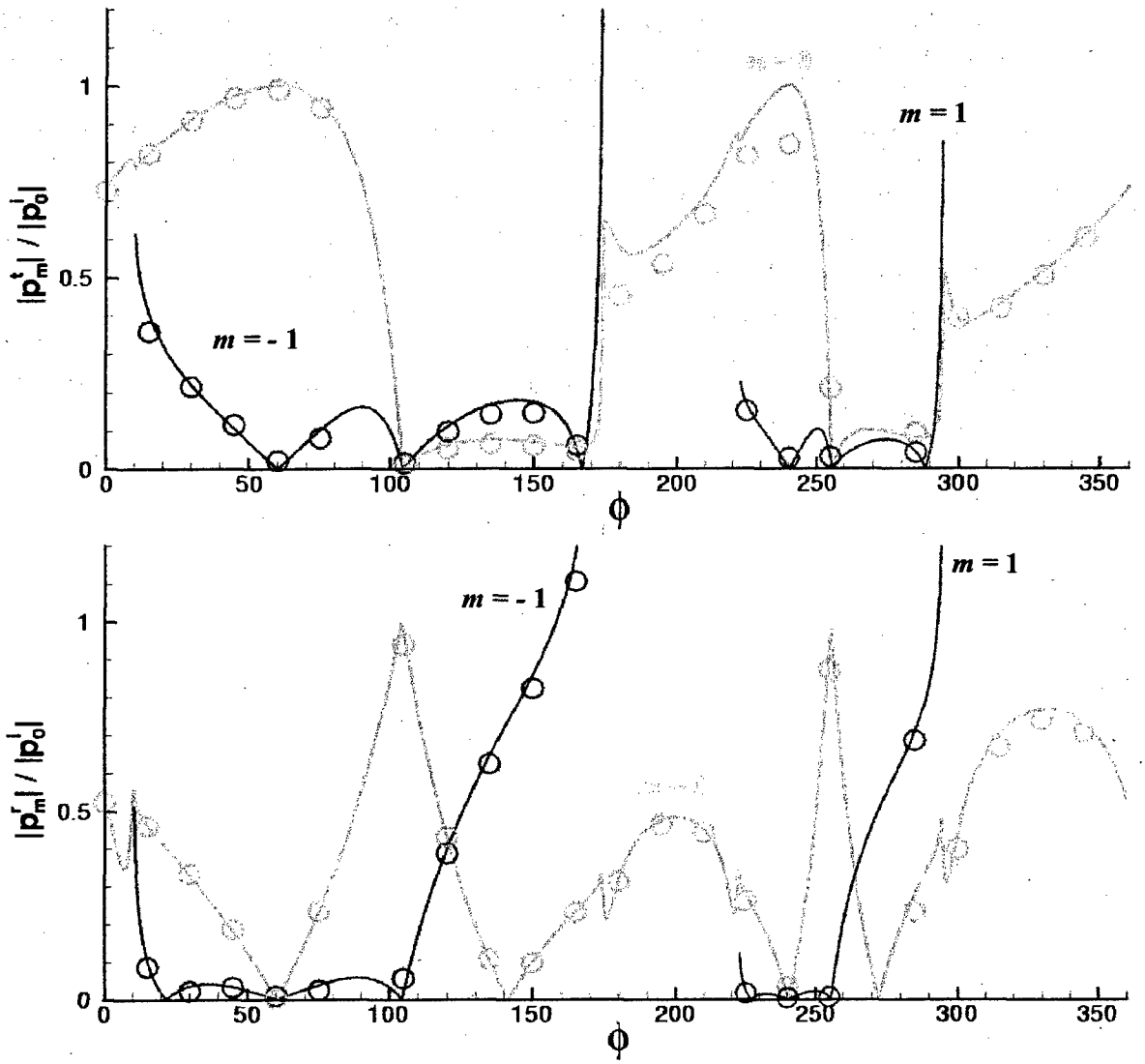

Figure 4.4: Variation of transmitted (top) and reflected pressures (bottom) with incidence angle for the super-resonant cases: Lines: analytical solution [5], ○ Lin3D.

6. Acknowledgement

The work described in this paper has been carried out in the framework of the research project 'Turbomachinery noise source CFD models for low noise aircraft designs - TurboNoiseCFD' funded by the European Commission within the GROWTH - 5th framework programme. The inspiration for this investigation came from the description of work of workpackage 1 and the authors are grateful to its workpackage leader A.G. Wilson for the fruitful discussions.

7. References

[1] Happel, H.-W. and Stubert, B.: Computation of Transonic 3D Cascade Flow and Comparison with Experiments, *AGARD-CP-437*, 1988.

[2] Kahl, G.: Application of the Time Linearized Euler Method to Flutter and Forced Response Problems, *ASME-95-GT-123*, 1995.

[3] Kahl, G. and Klose, A.: Time Linearized Euler Calculations for Unsteady Quasi-3D Cascade Flows, *6th Symp. on Unsteady Aerodynamics and Aeroelasticity in Turbomachines and Propellers*, Notre Dame, IN, Sept. 15-19, 1991.

[4] Kahl, G. and Klose, A.: Computation of Time Linearized Transonic Flow in Oscillating Cascades, *Int. Gas Turbine and Aeroengine Congress and Exposition*, Cincinnati, Ohio - May 24-27, *ASME-93-GT-269*, 1993.

[5] Koch, W.: "On the Transmission of Sound Waves through a Blade Row", Journal of Sound and Vibration, 18 (1) pp. 111-128 (1971).

[6] Wilson AG, 2000, *A Method for Deriving Tone Noise Information from CFD Calculations on the Aeroengine Fan Stage*, to be submitted for presentation at the NATO RTO-AVT Symposium on Developments in Computational Aero- and Hydro-Acoustics, Manchester, UK, 8-11 October 2001.